



Isotherm, Kinetic and Thermodynamic Studies of Mixed Metal Oxide Nanocomposite as an Efficient Adsorbent for Azo Dye Removal

Marziyeh Saati¹, Naiemeh Jarolmasjed¹, Hadi Pourradi², Kamellia Nejati¹, Arash Karimpour-Zahmatkesh³ and Samin Hamidi^{4*}

¹Department of Chemistry, Payame Noor University, Iran

²Department of Inorganic Chemistry, Tabriz University, Tabriz, Iran

³Faculty of Agriculture, Yasouj University, Yasouj, Iran

⁴Food and Drug Safety Research Center, Tabriz University of Medical Sciences, Iran

ABSTRACT

Azo dyes have been shown to damage ecosystems when discharged into water systems serious health risks to humans. This study has focused on the applications of nanomaterials in environmental remediation especially the treatment of industrial waste water and the polluted underground water. A low cost and effective adsorption method used for color removal from wastewater using a Ni-Al-Ce mixed metal oxide nanocomposite as an adsorbent for dye decontamination from wastewaters. The nanocomposite was prepared using the precipitation and calcination methods and fully characterized. As-prepared adsorbent was utilized for the sorption of Direct Red 23 (DR23), an azo dye, from the aqueous solutions. Furthermore, the adsorption of dye in a batch system was investigated according to different parameters such as pH and temperature with frequent sampling at time duration of 3 hr and their spectroscopic records were studied. Langmuir and Freundlich isotherms and two kinetic models of pseudo first-order and pseudo second-order were used to investigate the experimental data. In this study, the data have better correlation with the pseudo second-order kinetic equation and the Langmuir adsorption isotherm model. In addition, the reaction has endothermic chemisorption.

Keywords: Nanocomposite; Adsorption mechanism; Environmental safety; Dye removal

INTRODUCTION

Since the societies developed, people have been exposed to dye effluents. At present more than 9000 types of dyes have been incorporated in the color index and utilized in various areas such as textile, paper, plastics, printing, food processing, cosmetic industries, pharmaceuticals and dye manufacturing industries [1]. Dye manufacturing industries are the main sources leave large amount of discarded dyes which are very toxic and can cause serious ecological concerns. Having potable water necessitates the development of lots of innovative technologies and materials to overcome mentioned problems [2-4]. Dyes contain delocalized electron systems, like aromatic organic compounds with structures including aryl rings. The presence of chromophore groups changes colors to dyes which are radicals consisting of conjugated double bonds containing delocalized electrons. Other common chromophoric configurations include azo (-N=N-), carbonyl (=C=O), carbon (=C=C=), carbon-nitrogen (>C=NH or -CH=N-), nitroso (-NO or N-OH), nitro (-NO₂ or =NO-OH), and sulphur (C=S). The aromatic structure normally contains benzene, naphthalene, or anthracene rings, which are part of a chromogen-chromophore structure along with an auxochrome. The presence of ionising groups, known as auxochromes, results in a much stronger alteration of the maximum

absorption of the compound and provides bonding affinity. Some common auxochrome groups are $-NH_2$, $-COOH$, $-HSO_3$, and $-OH$. A detailed arrangement of the dyes and their structures is provided in the Colour Index (C.I.) [5]. There are several classes of synthetic dyes, such as azo, anthraquinone, metal complex, azo metal complex, and phthalocyanine. Among these categories, the type that has been mostly applied is azo dyes, which consists of one or more groups of azo ($-N=N-$) linked to an aromatic group [6], contain over 50% of all textile dyes, and have been widely used in many industries [7]. The dye structural designing is important because of its resistance to different degradation and destruction reactions, so that physical and chemical reactions are not capable of its demolition or elimination. Azo dyes are one of the main types of dye used by the textile industry. However, some azo dyes break down during use and release chemicals known as aromatic amines, some of which can cause health related problems [8]. Some azo dyes are toxic, mutagenic, and carcinogenic [9-11]. Thus common methods like coagulation, oxidation, electrochemical, ion-exchange, biodegradation, ultra-filtration, precipitation, ion exchange and reverse osmosis processes can't be used to remove this organic compound from the aqueous atmospheres formation of hazardous byproducts, high initial installation cost, generation of chemical wastes, and high-energy requirement [12-17]. Moreover, reductive fraction of one or more azo groups can produce a carcinogenic aromatic amine which is toxic for the animals and nature. Direct dyes are commonly used in the cotton and rayon, paper, leather, and, to some extent to nylon. They are water soluble anionic dyes. Generally the dyes in this group are polyazo compounds, along with some stilbenes, phthalocyanines and oxazines. There are several reports on removal of DR23 practically by adsorption which were listed in Table 1.

Table 1: DR23 removal by nano- and macro-sized adsorbents

a) nano sized adsorbents						
Adsorbent	Adsorbent dosage (g/L)	Dye concentration (mg/L)	pH	Temp. (°C)	Qm (mg/g)	Reference
Powdered tourmaline	1	16	3	25	153	[47]
CS-g-PNEANI copolymer	1	10	2	25	112	[39]
Activated carbon in a rotating packed bed (RPB)	-	50	-	-	8.35	[48]
ZFN-CTAB	0.4	50	2	25	26.1	[49]
Magnetic multi-walled carbon nanotubes-Fe ₃ C nanocomposite (MMWCNTs-ICN)	-	54	3.7	30	172.4	[50]
Polyaminoimide homopolymer (PAIHP)	0.005-0.02	300	2	25	5555	[51]
TiO ₂	-	650	<4.5		2.2-35.2	[52]
b) Macro sized adsorbents						
Adsorbent	adsorbent dosage (g/L)	dye concentration (mg/L)	pH	Temp. (°C)	Qm (mg/g)	Reference
Orange peel	2	50	2	25	10.72	[53,54]
Magnetic (barium ferrite)- chitosan beads	15	10	4	25	1250	[55]
Uncaria gambir (gambir)	-	-	2	30	26.67	[56]
Magnetic Corn stalk	0.2 g	90	3	25	27-52	[57]
Cationized wood sawdust	5	150	6.5	30	65.8	[58]
Untreated and activated rice husk by citric acid	-	25	-	25	2.41	[59]
Rhizophora apiculata bark	-	-	<7	30	21.6	[60]

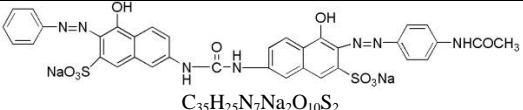
Azo dyes were banned by several countries due to their potential toxic nature [18]; so adsorption as a rapid phenomenon is one of the most beneficial techniques used for the elimination of dyes and other effluents from the aqueous/gaseous phase and their sorption on to the solid phase [19]. A large variety of adsorbents are used to remove dyes from the aqueous solutions [5,20-22]. Among the adsorption materials, inorganic compounds and metal oxides have been attracted much attention [23]. By combining of two or more

different materials, a composite material can be constructed that forms large regions to be regarded as continua, which are bonded together tightly at the interface. Many ingredients such as reinforced rubber, filled polymers, mortars and concrete alloys, porous and cracked media, aligned and chopped fibre composite, polystalline aggregate metals, etc., natural or artificial, are of this kind [24]. Lately, many researchers have been done on the nanocomposite materials. The combination of different compounds in nanoscale produces novel properties [25]. These properties bring out a variety of applications, amongst which, metal nanoparticles and metal-metal oxide composites are remarkable [26]. The purpose of the present research is to investigate the synthesis of Ni-Al-Ce nanocomposite on the basis of layered double hydroxide and to study the dye adsorption onto the nanocomposite. In the present work, we fabricated a novel Ce/Ni/Al nanocomposite to study its "green" removal potential in DR23 from aqueous solution. Investigating the mechanism of whole process was performed by Langmuir and Freundlich isothermic models as well as by the aid of two kinetically models of pseudo first-order and pseudo second-order.

EXPERIMENTAL SECTION

Nickel (II) Nitrate Hexahydrate ($\text{Ni}(\text{NO}_3)_2 \cdot 6\text{H}_2\text{O}$), Aluminum Nitrate Nonahydrate ($\text{Al}(\text{NO}_3)_3 \cdot 9\text{H}_2\text{O}$), Cerium (III) Nitrate Hexahydrate ($\text{Ce}(\text{NO}_3)_3 \cdot 6\text{H}_2\text{O}$) and other reagents used as received without further purification (all chemical reagents purchased from Merck and Sigma-Aldrich). Deionized water was used as solvent, in which was boiled and nitrogen saturated if needed, in order to prevent atmospheric CO_2 intercalation as carbonate anion presented in air exposed water [27]. DR23, was obtained from Boyakhsazan Co., Iran. The characteristics of DR23 dye were shown in Table 2.

Table 2: The characteristics of direct red 23

Chemical name	Chemical structure	Chemical class	Color index	λ_{max} (nm)	Mw (g/mol)
Direct Red 23	 $\text{C}_{35}\text{H}_{25}\text{N}_7\text{Na}_2\text{O}_{10}\text{S}_2$	Diazo class	29160	505	813.7

Synthesis of the Ni-Al-Ce Mixed Metal Oxide ($\text{NiO}/\text{Al}_2\text{O}_3/\text{CeO}_2$) Nanocomposite

The Ni-Al-Ce mixed metal oxides were synthesized by the co-precipitation method. $\text{Ni}(\text{NO}_3)_2 \cdot 6\text{H}_2\text{O}$ (0.870 g, 0.003 mol) and $\text{Al}(\text{NO}_3)_3 \cdot 9\text{H}_2\text{O}$ (0.375 g, 0.001 mol) with the $\text{Ni}^{2+}/\text{Al}^{3+}$ molar ratio of about 3 and $\text{Ce}(\text{SO}_4)_2 \cdot 4\text{H}_2\text{O}$ (0.404 g, 0.001 mol) were dissolved in 100 mL of deionized water. Then the pH of the solution was adjusted to 8.5 by the addition of NaOH solution (1 M) and Na_2CO_3 (2 M). The system was refluxed at 65°C for 24 h. The products were centrifuged at the speed of 3000 rpm for 10 min and the solid was washed thoroughly with deionized water and then dried at 50°C . The dried $\text{NiO}/\text{Al}_2\text{O}_3/\text{CeO}_2$ nanocomposite was calcined at 500°C for 18 h to change into Ni-Al-Ce mixed metal oxide nanocomposite [28].

Characterization Techniques

The FT-IR spectra were obtained using KBr disk method at room temperature with a Shimadzu 8400s spectrophotometer in the range of $4000\text{--}400\text{ cm}^{-1}$. The X-ray diffraction (XRD) pattern of the samples was taken by a Bruker D-8 Advance diffractometer with $\text{Cu K}\alpha$ radiation, between 4 and 80° , with 2θ step of 0.02° . The scanning electron microscope (SEM) images were taken using a Hitachi S 4160 with an acceleration voltage of 25 kV. Shimadzu UV-1601PC is the instrument with which the UV-Vis spectra were recorded in the range of $200\text{--}800\text{ nm}$.

Dye Solution Preparation

A stock solution of dye (1000 mg/L) was prepared by weighing the accurate amount of the dye dissolved in double distilled water. Solution prepared in the experiment for the target concentration obtained by dilutions. Dye concentration was calculated by using absorbance values measured before and after the treatment, at 510 nm with Shimadzu UV-1601PC. Experiments were carried out at initial pH value is 6.5 and was controlled by addition of sodium hydroxide or hydrochloric acid.

Adsorption Experiments

The adsorption performance was made by using 100 mL of a dye solution by diluting the stock solution to desired concentration and known amount of adsorbent was added to the solution and stirred vigorously for a predefined time. Experiments were conducted to evaluate the effect of various factors such as pH and temperature, with a univariate method. When the equilibrium was established, supernatant was carefully filtered through Whatmann filter paper (No. 1) saturated with distilled water. To further confirm the adsorption of dye on the filter, a comparative study was done by taking a known amount of the dye. Adsorption of dye on filter paper was not observed. The dye solution became colorless after filtration. For adjusting the pH value of the reacting solution, buffered solutions with pH values of 4-10 were used [29]. Desired pH values of the DR23 solutions were stabilized by adding the minimum amount of the buffered solutions before the addition of the nanocomposite; then 30 mg of the NiO/Al₂O₃/CeO₂ nanocomposite was dispersed in 100 mL of DR23, with the contact time 180 min and temperature of 20-65°C [30]. To estimate the concentration of sample from each experiment, a calibration curve of dye was first constructed. The removal percent and adsorbed amount of dye were recorded spectrophotometric measurements using a Shimadzu 1601-PC UV-Vis spectrophotometer absorbance of the sample solutions before and after removing process at appropriate wavelengths corresponding to the maximum absorbance which is 501 nm [31]. All the experiments were performed in triplicates and the results expressed as mean values. The following equation was applied to calculate the dye removal efficiency:

$$\% \text{Removal} = \left(\frac{C_0 - C_t}{C_0} \right) \times 100 \quad (1)$$

Where, C_0 and C_t are the initial and residual concentrations of dye in the solution (mg/L), respectively.

The procedures of kinetic experiments were performed at different contact times at temperatures of 293, 308, 323 and 338 K. The adsorption capacity, Q_t (mg/g), was calculated using equation (2):

$$Q_t = (C_i - C_t) V/M \quad (2)$$

in which C_i (mg/L) is the initial concentration of DR23, C_t (mg/L) is the concentration of DR23 at time t in the solution, V is the volume of the solution (L), and M is the mass of the adsorbent (g) [32]. To design an efficient adsorption performance for dye removal, it is important to implement the most appropriate correlation for the equilibrium curves. This equilibrium adsorption capacity curves can be obtained by calculating the adsorption isotherm of dyes onto the adsorbent. Two isotherm equations including Langmuir and Freundlich have been established in this investigation. For adsorption isotherm studies, dye solutions dye solution was agitated with known amount of adsorbent until the equilibrium was achieved and equilibrium adsorption capacity was calculated from the Q_e and at equilibrium point, (Q_e , mg/g) were calculated by the following equations, respectively:

$$Q_e = \frac{(C_i - C_e) \times V}{M} \quad (3)$$

with above mentioned C_i parameter, C_e (mg/L) being the DR23 concentration at equilibrium point, V (L) the volume of the dye solution and M (g) the mass of dry adsorbent [30,33].

RESULTS AND DISCUSSION

Characterization

The as-prepared nanocomposite was subjected to FT-IR spectroscopy as a useful instrument to characterize the certain functional groups in nanocomposite. As depicted in Figure 1, the bands at 665, 609, and 561 cm^{-1} indicate stretching mode of metal-O and metal-O-H bending vibrations [34]. The XRD pattern of NiO/Al₂O₃/CeO₂ nanocomposite which was calcinated is shown in Figure 2. After calcination, nanocomposite shows polycrystalline nature. The NiO and CeO₂ XRD patterns shown in Figure 2 have several additional peaks appeared at $2\theta \approx 29^\circ$, 33° , 37° , 48° and 56° , corresponding to the (2 0 0), (2 0 1), (2 2 0) and (3 1 1) reflections, respectively, but Al₂O₃ peaks are visible in $2\theta \approx 43^\circ$ and 64° as well. SEM images demonstrate the morphology of NiO/Al₂O₃/CeO₂ nanocomposite which was synthesized through calcination method. The CeO₂ particles were displayed by the white bulks [35] (Figure 3).

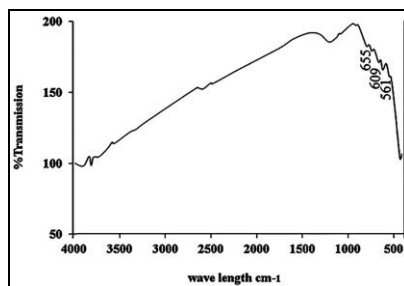


Figure 1: The FT-IR spectra of the nanocomposite

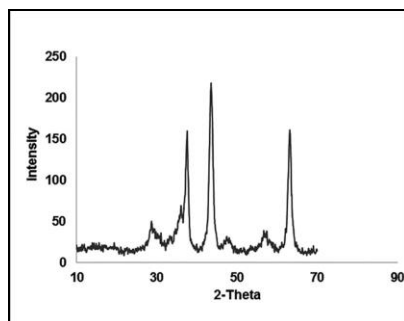


Figure 2: The XRD patterns of the nanocomposite

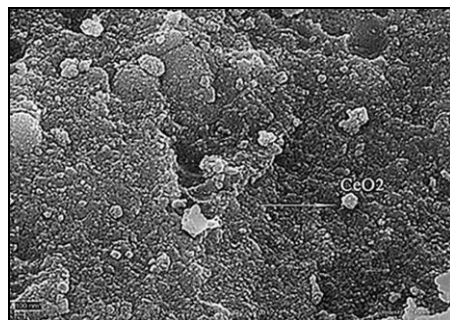
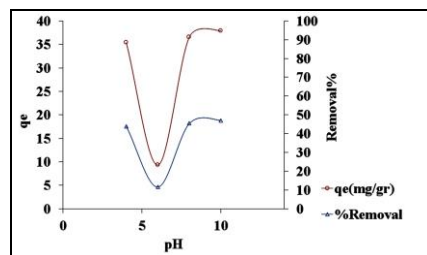


Figure 3: The SEM image of the nanocomposite

Figure 4: The effect of pH on DR23 adsorption by the nanocomposite. [DR23]=24 mg/L; adsorbent dosage=0.03 gL⁻¹; T=65°C; t=180 min)

Adsorption Experiment

The effect of pH:

The pH is one the most important parameters both aqueous chemistry and controlling the adsorption of dye on to the adsorbent. The effect of pH on the adsorption process was assessed in the range of 4-10 under the temperature of 338 K, contact time of 180 min and DR23 concentration of 3 mg/L. The surfaces of metal

oxides are generally covered with hydroxyl groups that vary in form with pH. Maximum adsorption value was investigated at pH 8.0. This result indicated that the adsorption capacity increased with increasing of initial solution pH [32,36,37]. Hence, all the next investigations were performed at pH 8 (Figure 4).

The effect of temperature:

Temperature has notable effects on the adsorption performance. As the temperature increases, rate of diffusion of dye molecules across the external boundary layer and internal pores of the adsorbent particle increases. Altering the temperature will cause changes in equilibrium point of the adsorbent for particular molecule [38]. According to the obtained data from Figure 5, the percentage of removal of DR23 by the nanocomposite increased with rising the temperature from 20°C to 65°C that indicates the endothermic nature of adsorption process.

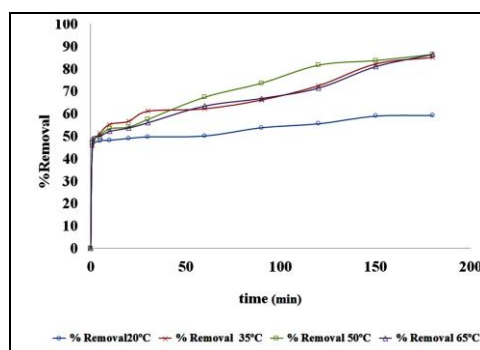


Figure 5: The percentage of removal of DR23 by the nanocomposite at different temperatures; pH=6 and other parameters are presented in Figure 4

Adsorption Kinetics:

Kinetic investigation the mechanism of adsorption that is crucial for the efficiency of the procedure. It is important to know the dye removal rate during adsorption set-up to optimize the system parameters. Thus, estimating the rate at which adsorption occurs for a given design is probably the most important factor in adsorption process design. To characterize adsorption process, the kinetic data were fitted with two empirical models namely the pseudo-first-order and the pseudo-second-order models.

In order to designate an appropriate adsorption system by investigation of rate and diffusion mechanisms belonging in the adsorption process, the Lagergren pseudo-first-order [39] and the Ho pseudo-second-order [40] diffusion kinetic models, were tested in which expressed by the following forms, respectively:

$$\text{Log}(q_e - q_t) = \text{log } q_e - (k_1/2.303)t \quad (4)$$

$$\frac{dq_t}{dt} = k_2(q_e - q_t) \quad (5)$$

Where, q_e (mg/g) and q_t (mg/g) represent the amounts of adsorbed DR 23 per unit mass of adsorbent at the equilibrium time (180 min here) and any other time, t (min). Also, the parameters k_1 (min^{-1}) and k_2 ($\text{g mg}^{-1} \text{min}^{-1}$) are the sorption rate constants of pseudo-first-order and pseudo-second-order models, respectively. The linear correlation coefficients (R^2) show the conformity between the experimental data and the model-predicted values. So, a relatively high R^2 value indicates a good accommodation between experimental data and the model assumption that subsequently shows the model success in describing the adsorption kinetic data. As results show in Table 3, the experimental data for the DR23 were better described by the pseudo-second order model, which presented the highest R^2 at the evaluated temperatures. The pseudo second-order plot for the adsorption of adsorbate on the adsorbent is shown in Figures 6 and 7. The linear plot results from the adsorption process that follows the pseudo second-order kinetics [41].

Table 3: The kinetic parameters and correlation coefficients (R^2) for the removal of DR23 (0.024 mg/L) by nanocomposite (0.03 g/L)

Temperature (K)	Pseudo first-order					Pseudo second-order		
	q_e exp (mg/g)	k_1 (min^{-1})	q_e cal (mg/g)	R^2	q_e exp (mg/g)	K_2 (g/mg.h)	q_e (mg/g)	R^2
293	143.016	0.008	5.96	0.861	143.01	0.007	142.85	1
308	205.508	0.008	8.87	0.832	205.8	0.004	204.081	0.98
323	208.805	0.01	9.1	0.929	208.8	0.004	212.76	0.99
338	208.806	0.008	9.33	0.792	208.8	0.004	208.33	0.98

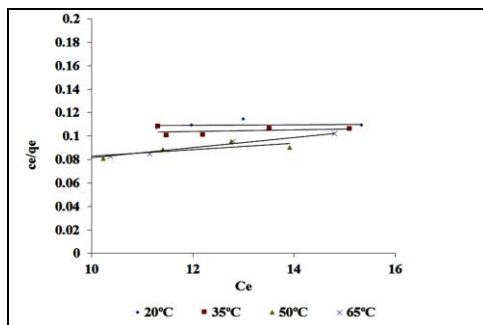


Figure 6: The pseudo first-order sorption plots for the DR23 sorption on the nanocomposite

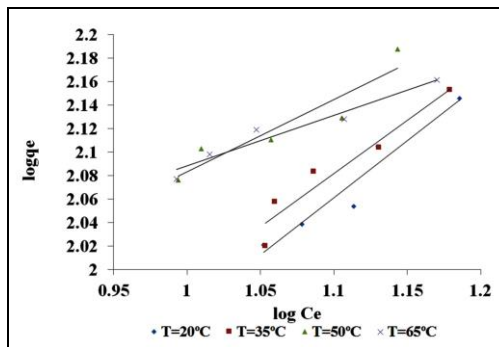


Figure 7: The pseudo second-order sorption plots for the DR23 sorption on the nanocomposite

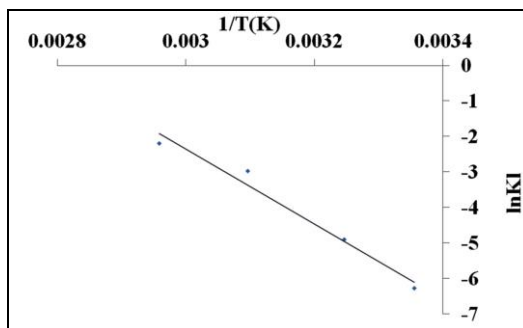


Figure 8: Langmuir isotherms for DR23 adsorption at temperature rates of 20, 35, 50, and 65°C

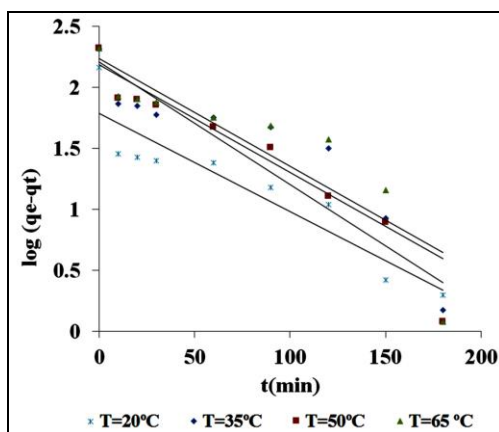


Figure 9: Freundlich isotherms for DR23 adsorption at temperature rates of 20, 35, 50, and 65°C

Adsorption Isotherm

The adsorption curves were used to both Langmuir and Freundlich equations. Langmuir's model of adsorption estimates the existence of monolayer coverage of the adsorbate at the outer surface of the adsorbant. The isotherm equation further evaluated by Freundlich equation that adsorption occurs at specific homogeneous places on the adsorbent, which implies that all adsorption sites are similar and energetically equivalent [42]. These isotherms are beneficial for estimating the total dose of adsorbent required to adsorb a required amount of adsorbate from solution. Langmuir and Freundlich isotherms are the most widely used methods for analyzing the experimental data through their linear form. The Langmuir isotherm shows that the layers of the adsorbent were adsorbed as the homogeneous mono-layer. The linear form of Langmuir equation is expressed as;

$$\frac{1}{q_e} = \frac{1}{q_m K_L C_e} + \frac{1}{q_m} \quad (6)$$

Q_m (mg/g) stands for the maximum amount of dye adsorbed per mass unit of the nanosorbant, C_e (mg/L) is the dye concentration, q_e (mg/g) is the amount of dye adsorbed per weight unit (mg) of the nanocomposite, which are all at equilibrium states, and K_L (L/mg) is the Langmuir constant related to the affinity of the binding sites. On the other hand, the adsorption that takes place on the heterogeneous adsorbent surface with uniform energy and Freundlich isotherm model can be expressed by following equation:

$$\log q_e = \log K_f + \frac{1}{n} \log C_e \quad (7)$$

where q_e (mg/g) and C_e (mg/L) are the same as explained before, K_f represents the adsorption capacity which is the Freundlich constant, and $(1/n)$ is the adsorption intensity. K_f can be defined as adsorption of distribution coefficient and represents the quantity of dye adsorbed onto adsorbent for an equilibrium concentration. The slope $1/n$, ranging between 0 and 1, is a measure of adsorption intensity or surface heterogeneity, becoming more heterogeneous as its value gets closer to zero [43]. Characteristic isotherm equations parameters (q_m , K_L , K_f , R_L , $1/n$) corresponding to Langmuir and Freundlich models together with R^2 values are summarized in Table 4. The results demonstrated that the adsorption of DR23 on the adsorbent was fit well with the Langmuir isotherm model with high R^2 value of 0.9983 compared to the Freundlich isotherm model ($R^2=0.9863$). It can be assumed that DR23 was adsorbed on surface of the adsorbent to achieve the complete monolayer coverage as indicated by Langmuir model. Figures 8 and 9 presented the adsorption isotherms of the dyes at pH 8.0.

^a q_m is the maximum adsorption capacity corresponding to complete monolayer coverage on the surface (mg/g).

^b K_L is the Langmuir constant (L/mg).

^c R^2 is correlation coefficient.

^d K_f is the Freundlich constant (L/mg).

n is adsorption intensity, $1/n$, ranging between 0 and 1, presented favorable adsorption.

Table 4: The Langmuir and Freundlich isotherm constants for the adsorption of DR23 by the nanosorbant

Temperature (K)	Langmuir isotherm			Freundlich isotherm		
	q_m^a (mg/g)	K_L^b (L/mg)	R^{2c}	K_f^d (mg/g)(L/mg) $^{1/n}$	n^e	R^2
293	5000	0.001	0.01	9.77	1.03	0.94
308	1428	0.007	0.11	12.02	1.1	0.93
323	375	0.05	0.69	29.12	1.16	0.87
338	232	0.11	0.98	45.65	2.33	0.94

Thermodynamic Studies

Thermodynamic parameters were assessed to confirm the adsorption nature and the inherent energetic changes involved during removal process. In order to determine whether a sorption process will occur spontaneously, thermodynamic parameters are applied. The standard enthalpy (ΔH°), the standard free energy (ΔG°) and the standard entropy (ΔS°) are three thermodynamic parameters to specify if the process is spontaneous or non-spontaneous, and endothermic or exothermic, using the following formula:

$$\ln K_L = \frac{\Delta S^\circ}{R} - \frac{\Delta H^\circ}{RT} \quad (8)$$

where R (8.314 J/mol K) represents the universal gas constant, T (K) stands for the absolute solution temperature, and K_L (L/mg) shows the Langmuir isotherm constant. In a Van't Hoff plot ($\ln K_L$ as a function of $1/T$) a straight line is obtained (Figure 10), and ΔH° and ΔS° were determined by the slope and then ΔG° and can be calculated using the following relation [44,45]:

$$\Delta G^\circ = -RT \ln K_L$$

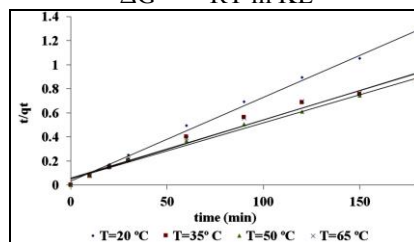


Figure 10: The Van't Hoff plot for the DR23 adsorption

The calculated thermodynamic parameters were shown in Table 5.

The non-spontaneity of the process can be determined from the adsorption data of DR23 on the nanocomposite [46]. The positive ΔH° which is greater than 87.58 kJ/mol shows the endothermic adsorption process; then the free energy change ΔG° and the ΔS° were obtained [41]. The positive value of ΔS° (534.03 J K⁻¹ mol⁻¹) suggests that the randomness at the solid/solution interface during the adsorption of DR23 on nanosorbent increases.

Table 5: Changes in Gibbs free energy, enthalpy, and entropy associated with the DR23 adsorption by the nano composite

(K) Temperature	$\ln K_L$	ΔG°	ΔH° (kJ/mol)	S^Δ
298	6.283-	15.566	87.58	243.1
308	4.910-	12.574		
323	2.981-	8.006		
338	2.197-	6.174		

CONCLUSION

Dyes are frequently used in various industries such as dyestuffs, textiles and leather. These dyes may pose dangerous carcinogenic and genotoxic effects. A broad range of conventional removal processes including coagulation, precipitation, membrane filtration, oxidation and adsorption have been developed for removing dyes from wastewater. These techniques are very expensive so it is necessary to develop the low cost sorbent compounds with high adsorption capacities. Proposed nanosorbent was found to be a promising sorbent for the removal of DR23 from aqueous solution, due to the removal efficacy, low cost and the fact that it can be used without previous treatment. The Langmuir model showed better fit and the estimated adsorbent capacity was 23.2 mg/g. The kinetics of process followed the pseudo-second-order model. The multilayer adsorption was proved by matching the data with the pseudo second-order kinetic equation. Adsorption isotherm provides both the qualitative information on the capacity of adsorbent and also the characteristic of the solute surface interaction.

The positive values of ΔG° , confirmed non-spontaneity of dye removal and positive value of enthalpy, ΔH° , showed the endothermic nature of sorption. To compare with commercial activated carbon, the proposed sorbent exhibits excellent performance for adsorption of anionic dyes.

REFERENCES

- [1] V Rocher; JM Siaugue; V Cabuil; A Bee. *Water Research*. **2008**, 42, 1290-1298.
- [2] M Perju; E Dragan. *Ione Exchange Letters*. **2010**, 3, 7-11.
- [3] K Singh; S Arora. **2011**, 41, 807-878.
- [4] MT Yagub; TK Sen; S Afroze; HM Ang. **2014**, 209, 172-184.
- [5] S Allen; B Koumanova. *J Univ Chem Tech Metallurgy*. **2005**, 40, 175-192.
- [6] S Song; H Ying; Z He; J Chen. *Chemosphere*. **2007**, 66, 1782-1788.
- [7] S Song; L Xu; Z He; H Ying; J Chen; X Xiao; B Yan. *J Hazardous Materials*. **2008**, 152, 1301-1308.
- [8] N Dom; D Knapen; D Benoot; I Nobels; R Blust. *Chemosphere*. **2010**, 81, 177-186.
- [9] KC Chen; JY Wu; CC Huang; YM Liang; SC J Hwang. *J Biotech*. **2003**, 101, 241-252.
- [10] Q Hu; Z Xu; S Qiao; F Haghseresht; M Wilson; GQ Lu. *J Colloid Interface Sci*. **2007**, 308, 191-199.
- [11] V Gupta. *J Env Manag*. **2009**, 90, 2313-2342.
- [12] E Razo-Flores; M Luijten; B Donlon; G Lettinga; J Field. *Water Sci Tech*. **1997**, 36, 65-72.
- [13] WW Ngah; L Teong; M Hanafiah. *Carbohydrate Polymers*. **2011**, 83, 1446-1456.
- [14] SK Nataraj; KM Hosamani; TM Aminabhavi. *Water Research*. **2006**, 40, 2349-2356.
- [15] S Raghu; CA Basha. *J Hazardous Mat*. **2007**, 149, 324-330.
- [16] M-X Zhu; L Lee; H-H Wang; Z Wang. *J Hazardous Mat*. **2007**, 149, 735-741.
- [17] MS Siboni; M Samarghandi; J-K Yang; S-M Lee. *J Adv Oxid Tech*. **2011**, 14, 302-307.
- [18] M Mitchell; WR Ernst; GR Lightsey; ET Rasmussen; P Bagherzadeh. **1978**, 19, 307-311.
- [19] Y Anjaneyulu; NS Chary; DSS Raj. *Reviews in Environmental Science and Bio/Technology*. **2005**, 4, 245-273.
- [20] E Forgacs; T Cserhati; G Oros. *Env Int*. **2004**, 30, 953-971.
- [21] SV Mohan; NC Rao; J Karthikeyan. *J Hazardous Mat*. **2002**, 90, 189-204.
- [22] H Kaşgöz; A Durmus. **2008**, 19, 838-845.
- [23] G Crini. *Bioresource Tech*. **2006**, 97, 1061-1085.
- [24] Z Hashin. *J Appl Mech*. **1983**, 50, 481-505.
- [25] BS Reddy. *InTech*. **2011**.
- [26] K Richter; A Birkner; AV Mudring. *Angewandte Chemie International Edition*. **2010**, 49, 2431-2435.
- [27] H Xiao; Z Ai; L Zhang. *The J Phys Chem C*. **2009**, 113, 16625-16630.
- [28] Z Rezvani; M Sarkarat; A Khataee; K Nejati. *Cry ResTech*. **2012**, 47, 1172-1184.
- [29] CJ Luk; J Yip; CM Yuen; C Kan; K Lam. *J Fiber Bioeng Info*. **2014**, 7, 35-52.
- [30] A Chaparadza; JM Hossenlopp. *J Colloid Interface Sci*. 2011, **363**, 92-97.
- [31] N Sobana; K Selvam; M Swaminathan. *Separation and Purification Technology*. **2008**, 62, 648-653.
- [32] K Nejati; S Davary; M Saati. *Appl Surface Sci*. **2013**, 280, 67-73.
- [33] S Nethaji; A Sivasamy; G Thennarasu; S Saravanan. *J Hazardous Mat*. **2010**, 181, 271-280.
- [34] NT McDevitt; WL Baun. *Spectrochimica Acta*. **1964**, 20, 799-808.
- [35] JS Valente; F Tzompantzi; J Prince. *Appl Catal B: Env*. **2011**, 102, 276-285.

- [36] W Somboon; P Mutitamongkol; P Tanpaiboonkul. Removal of colored wastewater wastewater generated from hand-made textile weaving industry. **2010**.
- [37] V Venkateswaran; V Priya; P Balasubramaniam. *Chem Sci Trans.* **2013**, 2, 771-780.
- [38] Z Al-Qodah. *Water Research.* **2000**, 34, 4295-4303.
- [39] M Abbasian; M Jaymand; P Niroomand; A Farnoudian-Habibi; SG Karaj-Abad. *Int J Biol Macromol.* **2017**, 95, 393-403.
- [40] YS Ho; G McKay. *Process Biochemistry.* **1999**, 34, 451-465.
- [41] Y Ho; G McKay. *The Canadian J Chem Engg.* **1998**, 76, 822-827.
- [42] W Cheung; Y Szeto; G McKay. *Bioresource Tech.* **2009**, 100, 1143-1148.
- [43] G Mckay; H Blair; J Gardner. *J Appl Polymer Sci.* **1982**, 27, 3043-3057.
- [44] A Rahmani; HZ Mousavi; M Fazli. *Journal of Water Resource and Protection.* **2010**, 253, 94-100.
- [45] MA Ahmad; R Alrozi. *Chem Engg J.* **2011**, 171, 510-516.
- [46] WW Ngah; M Hanafiah. *Biochem Engg J.* **2008**, 39, 521-530.
- [47] N Liu; H Wang; CH Weng; CC Hwang. *Arabian J Chem.* **2016**.
- [48] A Kundu; LS Hassan; G Redzwan; D Robinson; MA Hashim; B SenGupta. *Desalin Water Treat.* **2016**, 57, 13518-13526.
- [49] NM Mahmoodi; J Abdi; D Bastani. *J Env Health Sci Engg.* **2014**, 12, 96.
- [50] W Konicki; I Pelech; E Mijowska; I Jasińska. *Chem Engg J.* **2012**, 210, 87-95.
- [51] NM Mahmoodi; F Najafi; S Khorramfar; F Amini; M Arami. *J Hazardous Materials.* **2011**, 198, 87-94.
- [52] PJ Holliman; BV Velasco; I Butler; M Wijdekop; DA Worsley. *Int J Photoener.* **2008**, 2008.
- [53] M Arami; NY Limaee; NM Mahmoodi; NS Tabrizi. *J Colloid Interface Sci.* 2005, **288**, 371-376.
- [54] FD Ardejani; K Badii; NY Limaee; N Mahmoodi; M Arami; S Shafaei; A Mirhabibi. *Dyes and Pigments.* **2007**, 73, 178-185.
- [55] SH Sanlier; G Ak; H Yilmaz; G Ozbakir; O Cagliyan. *Preparative Biochemistry and Biotechnology.* **2013**, 43, 163-176.
- [56] A Achmad; J Kassim; TK Suan; RC Amat; TL Seey. *J Phys Sci.* **2012**, 23, 1-13.
- [57] M Fathi; A Asfaram; A Farhangi. *Spectrochimica Acta Part A: Molecular and Biomolecular Spectroscopy.* **2015**, 135, 364-372.
- [58] A Hebeish; MA Ramadan; E Abdel-Halim; A Abo-Okeil. *Clean Technologies and Environmental Policy.* **2011**, 13, 713-718.
- [59] O Abdelwahab; A El Nemr; A El Sikaily; A Khaled. *Egyptian J Aqua Res.* **2005**, 31, 1-11.
- [60] L Tan, K Jain, C Rozaini. *J of Appl Sci Env San.* **2010**, 5.